Report

Current Biology

The BES1/BZR1-family transcription factor MpBES1 regulates cell division and differentiation in *Marchantia polymorpha*

Graphical abstract

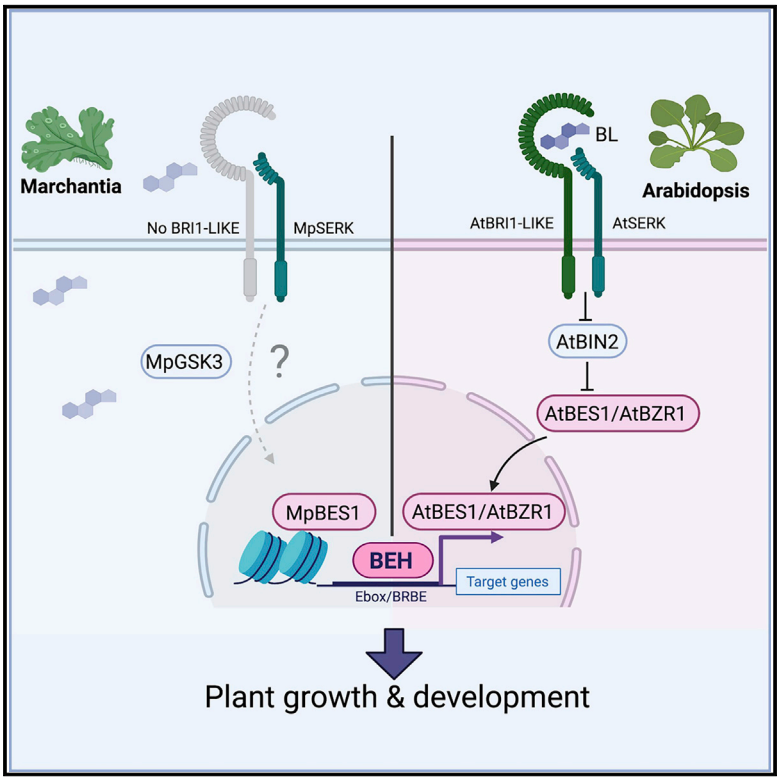

Authors

Martin A. Mecchia,
Mariano García-Hourquet,
Fidel Lozano-Elena, ...,
Mar Marquès-Bueno,
Santiago Mora-García,
Ana I. Caño-Delgado

Correspondence

ana.cano@cragenomica.es

In brief

In angiosperms, brassinosteroids regulate cell growth through the post-translational control of BEH transcription factors. Mecchia, García-Hourquet, et al. show that MpBES1, the closest BEH homolog in *Marchantia polymorpha*, plays a crucial role in cell division and differentiation, even if brassinosteroid signaling is apparently absent in liverworts.

Highlights

- MpBES1 is the closest homolog of angiosperm BEH proteins in *Marchantia polymorpha*
- MpBES1 plays a key role in meristem cell division and differentiation in Marchantia
- MpBES1 behaves as a gain-of-function form when expressed in *Arabidopsis thaliana*
- BR signaling likely co-opted this module, introducing new regulatory checkpoints

Mecchia et al., 2021, Current Biology *31*, 4860–4869
November 8, 2021
https://doi.org/10.1016/j.cub.2021.08.050

CellPress

CellPress

Current Biology

Report

The BES1/BZR1-family transcription factor MpBES1 regulates cell division and differentiation in *Marchantia polymorpha*

Martin A. Mecchia,[1,3,4] Mariano García-Hourquet,[2,4] Fidel Lozano-Elena,[1] Ainoa Planas-Riverola,[1] David Blasco-Escamez,[1] Mar Marquès-Bueno,[1] Santiago Mora-García,[2,5] and Ana I. Caño-Delgado[1,5,6,7,*]

[1]Department of Molecular Genetics, Centre for Research in Agricultural Genomics (CRAG) CSIC-IRTA-UAB-UB, Campus UAB (Cerdanyola del Vallès), 08193 Barcelona, Spain

[2]Fundación Instituto Leloir, IIBBA-CONICET, Buenos Aires, Argentina

[3]Present address: Department of Plant and Microbial Biology, University of Zurich, Zurich, Switzerland

[4]These authors contributed equally

[5]These authors contributed equally

[6]Twitter: @Ana_CanoDelgado

[7]Lead contact

*Correspondence: ana.cano@cragenomica.es

https://doi.org/10.1016/j.cub.2021.08.050

SUMMARY

Brassinosteroids (BRs) play essential roles in growth and development in seed plants;[1] disturbances in BR homeostasis lead to altered mitotic activity in meristems[2,3] and organ boundaries[4,5] and to changes in meristem determinacy.[6] An intricate signaling cascade linking the perception of BRs at the plasma membrane to the regulation of master transcriptional regulators belonging to the BEH, for BES1 homologues, family[7] has been described in great detail in model angiosperms. Homologs of these transcription factors are present in streptophyte algae and in land plant lineages where BR signaling or function is absent or has not yet been characterized. The genome of the bryophyte *Marchantia polymorpha* does not encode for BR receptors but includes one close ortholog of *Arabidopsis thaliana* BRI1-EMS-SUPPRESSOR 1 (AtBES1)[8] and *Arabidopsis thaliana* BRASSINAZOLE-RESISTANT 1 (AtBZR1),[9] MpBES1. Altered levels of MpBES1 severely compromised cell division and differentiation, resulting in stunted thalli that failed to differentiate adult tissues and reproductive organs. The transcriptome of Mp*bes1* knockout plants revealed a significant overlap with homologous functions controlled by AtBES1 and AtBZR1, suggesting that members of this gene family share a subset of common targets. Indeed, MpBES1 behaved as a gain-of-function substitute of AtBES1/AtBZR1 when expressed in *Arabidopsis*, probably because it mediates conserved functions but evades the regulatory mechanisms that native counterparts are subject to. Our results show that this family of transcription factors plays an ancestral role in the control of cell division and differentiation in plants and that BR signaling likely co-opted this function and imposed additional regulatory checkpoints upon it.

RESULTS AND DISCUSSION

MpBES1 is a bona fide homolog of angiosperm BEH proteins

To understand the ancestral function of the BES1 homologues (BEH) family, we set to characterize the closest homolog to *Arabidopsis thaliana* BRI1-EMS-SUPPRESSOR 1 (AtBES1)/*Arabidopsis thaliana* BRASSINAZOLE-RESISTANT 1 (AtBZR1) in the liverwort *Marchantia polymorpha* (Marchantia). Although traces of BR biosynthetic intermediates have been identified in Marchantia,[10] no clear physiological effects of these compounds have been reported and, moreover, liverworts lack BRL-type sequences.[11,12] In fact, we have not observed any phenotypic changes in Marchantia gemmalings treated with brassinolide or the brassinosteroid (BR)-biosynthesis inhibitor brassinazole (BRZ) (Figure S1A). We searched for BEH-related sequences in the genomes of streptophyte algae and representative species of land plants (Figures 1A and 1B), based on the conservation of diagnostic positions in the N-terminal DNA binding domain (DBD), a variant of the basic helix-loop-helix (bHLH) motif that characterizes the family.[13] BEH proteins clustered into three main branches. Branch I included the BR-regulated BEHs in angiosperms and related sequences in other plant lineages, including one member in Marchantia, Mp1g13260, named here MpBES1. Branches II and III grouped related but less characterized sequences, including the BZR1-β-amylase (BAM) proteins that, in addition to the DBD, contain a C-terminal BAM-like domain (Figure 1A).[14]

The DBD sequences are highly conserved in all members of branch I. Remarkably, a Cys residue whose oxidation state is functionally relevant in AtBZR1 and AtBES1[15] is also present in homologs from Zygnematales, the group of streptophyte algae

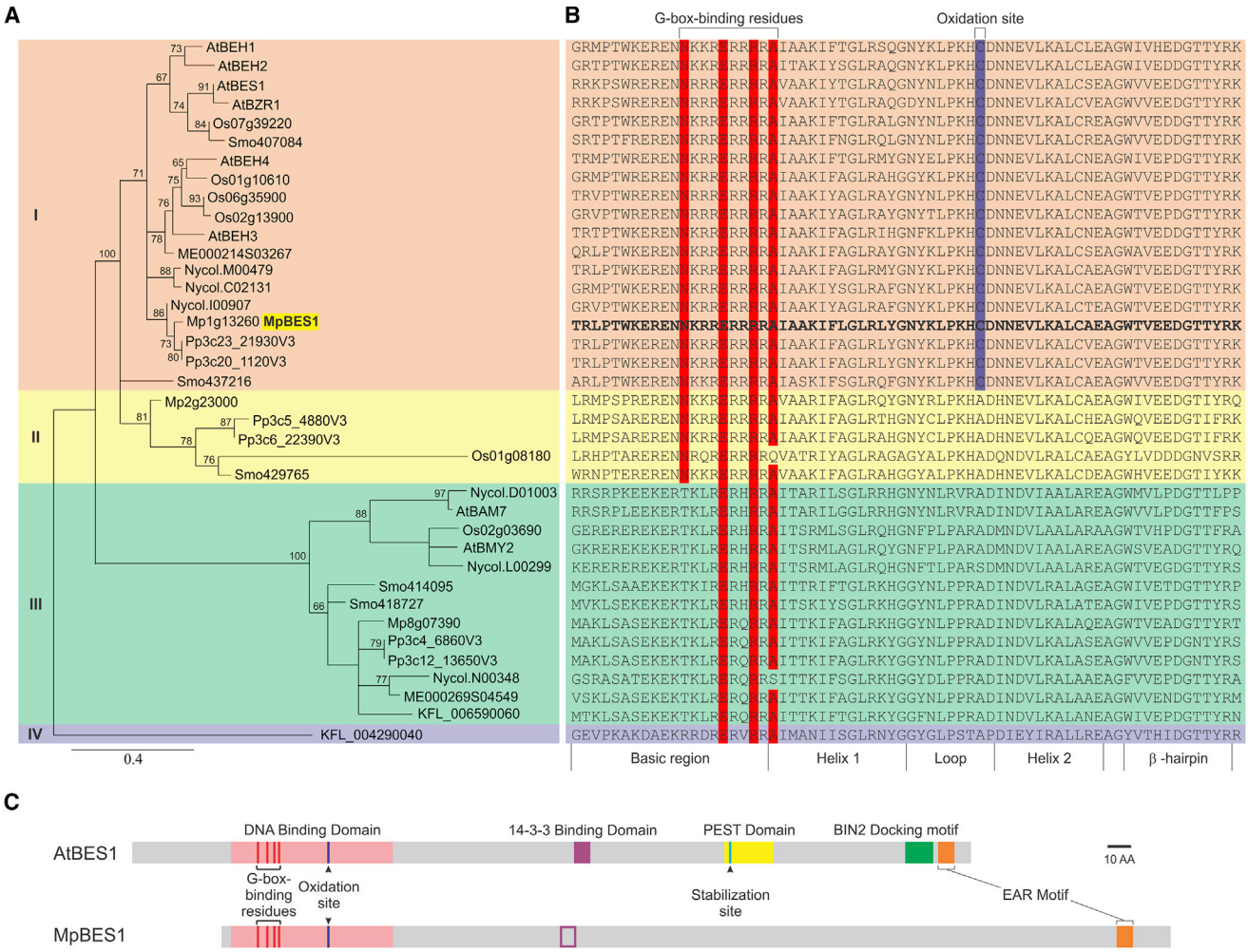

Figure 1. The BEH family in *Streptophyta*

(A) A rooted maximum likelihood tree of amino acid sequences of BEH family members in streptophytes. Sequences from the land plants *Marchantia polymorpha* (Mp), *Physcomitrella patens* (Pp), *Selaginella moellendorffii* (Selmo), *Nymphaea colorata* (Nyco), *Oryza sativa* (Os), and *Arabidopsis thaliana* (At) and the algae *Mesotaenium endlicherianum* (ME) and *Klebsormidium nitens* (KFL) were aligned using ClustalW. The numbers indicate the bootstrap values (%) from 1,000 replicates. MpBES1 is highlighted in bold type.

(B) Amino acid alignment of the basic helix-loop-helix DNA binding domain in the proteins displayed in (A). G-box binding amino acids are highlighted in red, and the Cys residue characteristic of sequences in branch I is highlighted in blue.

(C) Schematic representation of the primary structure of AtBES1 and MpBES1. Known AtBES1 motives and their homologous positions in MpBES1 are indicated.

more closely related to the ancestors of land plants (Figure 1B). In the C-terminal domain, two highly conserved motives can be also considered diagnostic of this branch. One of them overlaps with the 14-3-3 binding site in *Arabidopsis* and rice BZR1,[16,17] although the basic amino acid required for interaction with 14-3-3 proteins is only present in angiosperms. At the C terminus, all members bear an ethylene-responsive, element-binding-factor-associated amphiphilic repression (EAR) motif, which suggests that interaction with Groucho/Tup1-type co-repressors is an ancestral feature of this protein clade.[18,19] Neither the PEST/destabilization domain[8,20] nor the BRASSINOSTEROID INSENSITIVE 2 (BIN2) (AtSK21) docking motif[21] found in angiosperms is present in bryophytes (Figure 1C). We therefore focused on MpBES1, the closest homolog to AtBES1/AtBZR1.

MpBES1 promotes cell proliferation and differentiation in meristems

To investigate the biological function of MpBES1, we generated knockout lines using CRISPR-Cas9. We obtained several independent lines targeting a gRNA to the 3′ end of the DBD coding sequence (Figures 2A and S1B–S1D).

Thalli of all confirmed mutants displayed severe developmental defects and a dramatically reduced size (Figure 2B). Given the extreme phenotype of the knockout mutants, we also generated knockdown lines using an artificial microRNA (*amiR*-MpBES1; Figure S1E). Constitutive expression of the mature *amiR*-MpBES1 significantly reduced Mp*BES1* mRNA levels (Figure S1D) and also produced dwarfed plants resembling the CRISPR-Cas9 mutants (Figures 2B and S1E).

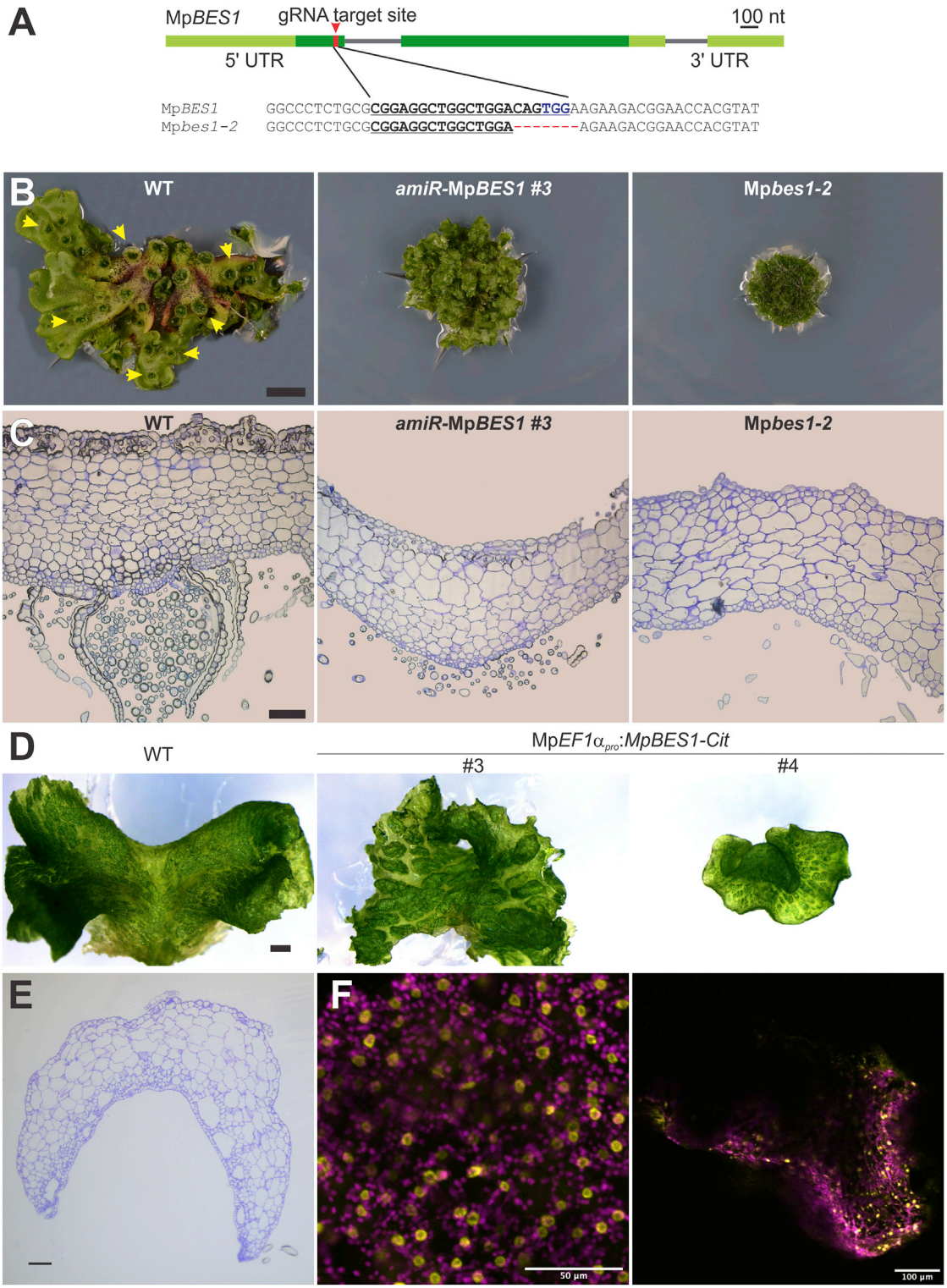

Figure 2. Changes in the expression levels of Mp*BES1* severely disrupt developmental processes in Marchantia

(A) Generation of knockout alleles of Mp*BES1* by CRISPR-Cas9. Exons are represented with boxes (coding sequence in dark green) and introns with lines; the gRNA target site is shown in red. WT and edited Mp*bes1-2* sequences are shown. See also Figure S1C for details on other independent knockout lines.

(B) Growth of Mp*BES1* loss-of-function mutants is severely affected. Images of 1-month-old WT, *amiR*-Mp*BES1* no. 3 knockdown, and Mp*bes1-2* knockout plants are shown; yellow arrows indicate gemma cups in the WT. Scale bar, 1 cm. See also Figures S1B, S1E, S2A, and S2B for further details on the phenotypes of these and other knockout and knockdown lines.

(legend continued on next page)

Mp*bes1-2* and *amiR*-Mp*BES1 no. 3* lines were selected for further characterization.

Knockout and knockdown plants were significantly smaller than the wild-type (WT) Tak-1 and failed to follow the dichotomic growth pattern typical of thalloid liverworts; instead, they produced compact thalli (Figure 2B). Although these lines were able to produce rhizoids, they never differentiated gemma cups and gemmae, nor were they able to produce antheridiophores when exposed to far-red light (Figure S2A). Histological transverse sections showed a severe reduction (*amiR*-Mp*BES1 no. 3*) or complete absence (Mp*bes1-2*) of areolae, air chambers or air pores in the dorsal surface; still, these lines produced an epidermal layer with elongated cells resembling those found in the WT plastochron I stage (Figures 2C and S2B).[22] The mutants did not produce ventral scales or bundled rhizoids, and the thalli consisted mainly of parenchymatous tissue (Figure 2C). Impaired MpBES1 function thus disrupted the differentiation between a photosynthetic dorsal layer and a storage ventral layer. Strikingly, the parenchyma cells in the mutants were larger than in the WT (Figure 2C). Because the mutant thalli were smaller, the total number of cells must accordingly be reduced. These features suggest that the balance between cell sizing, division, and expansion has been altered in the Mp*bes1* mutants that, as a result, mount a compensatory response with fewer but bigger cells. This phenomenon has been repeatedly observed in cell-proliferation-defective mutants in animals and plants.[23]

The shape of the thallus was also affected in overexpressing Mp*EF1*α_{pro}:Mp*BES1-Citrine* lines (Figures 2D and S2C). The phenotypic effects correlated with the amount of protein (Figure S2D). Planar growth and dorsoventrality were disrupted in overexpressing lines. These plants were able to differentiate air pores, albeit with an altered morphology, but they failed to produce gemmae (Figure 2E). Fluorescence was ubiquitously observed in nuclei, yet the protein appeared to accumulate preferentially at the growing edges of the thallus (Figure 2F). Taken together, these results show that imbalanced MpBES1 expression disrupts growth and differentiation.

In Marchantia, meristematic regions are located in notches at the apex of each ramification. A single stem cell divides in four planes to produce dorsal, ventral, and bilateral merophytes that proliferate and differentiate in response to local cues as they become separated from the meristem.[24] To take a closer look at the meristematic regions, we stained proliferating nuclei in 3-day-old gemmae of WT and of a β-estradiol-inducible *amiR*-MpBES1 line (*amiR*-Mp*BES1*^{ind}; Figures S2E and S2F) with 5-ethynyl-2′-deoxyuridine (EdU) (Figure 3A). Induced expression of the *amiR*-Mp*BES1* led to a reduced number of cells at the notches undergoing DNA duplication (Figures 3A and 3B) and an increased proportion of gemmae with only one active meristem (Figure 3C). We also mutated Mp*BES1* using CRISPR-Cas9 in a line expressing luciferase (LUC) under the control of the Mp*PRR* promoter, which is active in meristematic regions.[25] LUC activity was detected in and at the immediate vicinity of the apical notches in WT lines but at higher levels and along the edges of the thallus in Mp*bes1* knockouts, suggesting a delocalization of cells with meristematic identity in the mutants (Figure 3D). Taken together, our results show that, when the function of MpBES1 is impaired, merophyte proliferation is reduced and, at the same time, more cells dwell in an indeterminate state, which ultimately delays or prevents differentiation.

MpBES1 and AtBES1 share a set of common targets and functional properties

We evaluated the transcriptional alterations in Mp*bes1* mutants through RNA sequencing (RNA-seq) of 2-week-old WT and mutant regenerating thalli. We found 3,246 deregulated genes in the mutant (|fold-change| > 1.5; false discovery rate [FDR] < 0.05). In both up- and downregulated genes, the biological process more consistently enriched was ''oxidation-reduction processes'' (Figure 4A). A similar effect was observed in mutants for another plant-specific transcription factor that modulates cell proliferation, MpTCP1, a P-type member of the plant-specific TEOSINTE BRANCHED1/CYCLOIDEA/PROLIFERATING CELL NUCLEAR ANTIGEN FACTOR1 (TCP) family.[26] Whether this redox signal is a direct effect of the absence of MpBES1 or an indirect response caused by the inability to grow remains an open question. GO-term analysis also showed a significant enrichment in biological processes related to cell wall organization and carbohydrate metabolism (Figure 4A). Indeed, AtBZR1 and AtBES1 regulate the expression of many genes involved in cell wall remodeling,[27] a process of significant impact on cell division and elongation. Moreover, among the deregulated genes in Mp*bes1-2* with clear *Arabidopsis* homologs (2,456 genes out of 3,246, based on Phytozome annotation), we found a large over-representation of described direct targets of AtBES1 and AtBZR1 (Figure 4B).[28,29]

It has been long known that BRs regulate cell division.[2,30] Separation between lateral organs in angiosperms relies in part on the restriction of BR signaling and cell proliferation at the boundary between the emerging organ and the meristem.[4,5,31] In rice, BR-controlled expression of U-type cyclins in the abaxial surface of lamina joints determines the leaf bending angle,[32] and in *Arabidopsis*, the expression of D-type cyclins is regulated by BRs.[33] Correlating with the cell proliferation defects described, the D-type cyclin Mp1g24670 and the U-type cyclins Mp7g06850 and Mp3g25260 were significantly downregulated in the Mp*bes1* mutant (Figure S3A).

We also searched for DNA motifs in sequences upstream of the deregulated genes and found that a G-box with the canonical CACGTG sequence and a 3′ extension, akin to the BR binding

(C) Loss of function of Mp*BES1* prevents differentiation into adult tissues. Transversal sections of 1-month-old WT, *amiR*-Mp*BES1* no. 3 knockdown, and Mp*bes1-2* knockout plants are shown. Dorsal surface is up. Scale bar, 100 μm.

(D) Overexpression of Mp*BES1* also disrupts growth. Shown are fragments of WT and two independent Mp*EF1*α_{pro}:Mp*BES1-Citrine* lines. Scale bar, 1 mm. See also Figure S2C for the phenotype of other independent overexpressing lines.

(E) Overexpression of Mp*BES1* disrupts differentiation of adult tissues. Transversal sections of 1-month-old MpBES1ox no. 4 plants is shown. Scale bar, 100 μm (left panel).

(F) MpBES1:*Citrine* is ubiquitously found in the nuclei (left panel) but preferentially accumulates in the growing edges of thalli (right panel). Epifluorescence images of Mp*EF1*α_{pro}:Mp*BES1-Citrine* no. 4 line are shown.

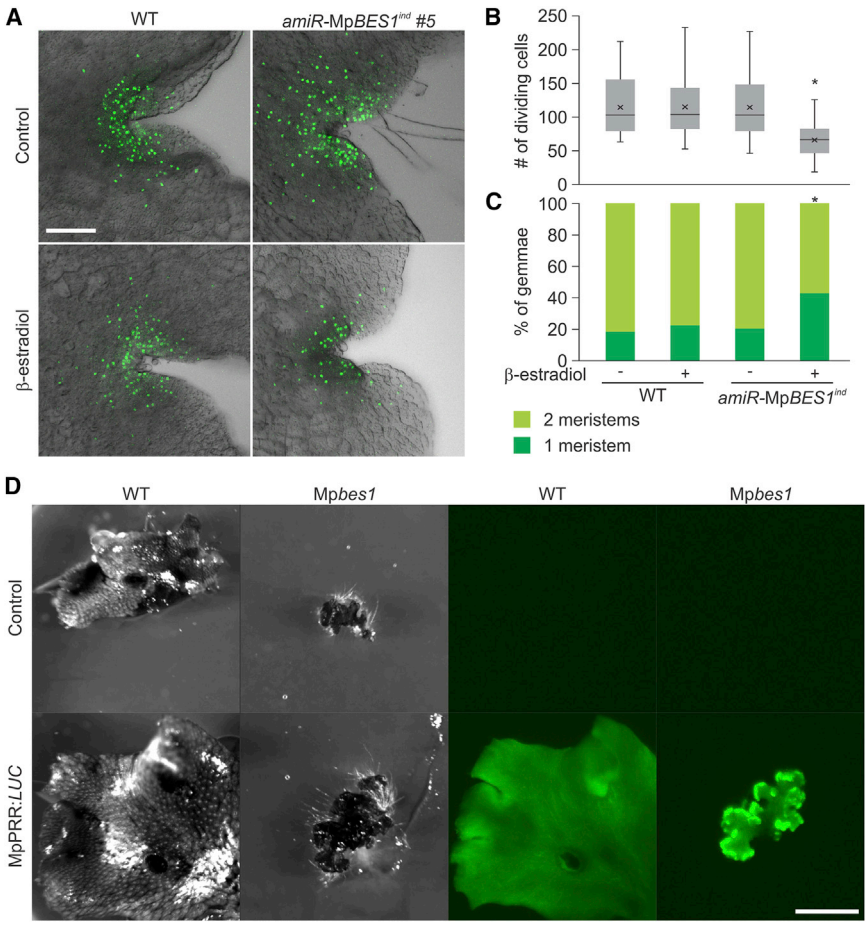

Figure 3. MpBES1 promotes cell proliferation and restricts meristematic niches

(A) Cell proliferation is impaired when the expression of Mp*BES1* is silenced. EdU staining in 3-day-old WT and *amiR*-Mp*BES1*^{ind} no. 5 gemmae is shown, untreated (upper panels) or treated with β-estradiol (lower panels) to induce the expression of the amiRNA (scale bar represents 100 μm). See also Figures S2E and S2F for phenotype and responses of *amiR*-Mp*BES1*^{ind} lines to β-estradiol.

(B) Quantification of the number of stained nuclei in meristematic notches, a proxy for mitotic activity, in WT and amiR-Mp*BES1*^{ind} no. 5 gemmae. n = 30; Student's t test; *p < 0.05.

(C) Silencing of Mp*BES1* leads to a higher proportion of localized meristem collapse. Proportion of 3-day-old gemmae with one or two discernible meristematic notches is shown. n = 30; Fisher's test; *p < 0.01.

(D) Loss of function of Mp*BES1* causes delocalization of meristematic regions. WT and Mp*bes1-2* knockout line (upper panels) and Mp*PRR*$_{pro}$*:LUC* WT and Mp*PRR*$_{pro}$*:LUC*/Mp*bes1-7* CRISPR-Cas9 lines (lower panels) were imaged under bright field (left panels) or under a charge-coupled device (CCD) camera after treating with D-luciferin (right panels; scale bar represents 1 cm).

element (BRBE) defined in *Arabidopsis*,[13,14,34] was significantly enriched only among upregulated genes (Figure S3B). These results suggest that MpBES1 is able to both activate and repress transcription, a feature shared with AtBES1 and AtBZR1; to the extent deregulated genes include its direct targets, MpBES1 may possibly have a more direct effect in transcriptional repression, which is congruent with the more populated set of common targets with AtBZR1 (Figure 4B).[34] In fact, MpBES1 was able to repress the expression of a LUC reporter expressed under the control of a concatemerized BRBE[35] and to activate transcription in yeasts binding to a fragment of the *AtCPD* promoter as efficiently as AtBZR1 or AtBES1, demonstrating that these proteins can bind to the same elements and operate similar responses (Figures S3C and S3D).

Given the apparent functional similarities between MpBES1 and AtBES1 and AtBZR1, we expressed MpBES1 in *Arabidopsis*. Independent transgenic lines displayed a range of phenotypes (Figure 4C) that correlated with the amount of MpBES1 protein (Figure S4A), which localized mainly in the nucleus (Figure S4B). Plants with the stronger phenotype had curled leaves, stem bends at the cauline leaf insertion site (Figure 4C, inset), and a significant delay in flowering, features also found in At*bes1-D* dominant mutants (Figure 4C). The overall phenotype of Mp*BES1*-overexpressing plants was reminiscent of plants overexpressing the gain-of-function At*bes1-D* (Figure S4C), At*bzr1-D*mEAR (where the EAR domain was replaced by the artificial transcriptional repression domain SRDX),[36] or AtBZR1Δ (where the 14-3-3 recognition site was deleted).[16] Accordingly, the lines expressing higher levels of MpBES1 were almost as tolerant to BRZ as At*bzr1-D* plants, and the expression levels of BR-regulated genes were also similar to what is found in At*bzr1-D* mutants, showing that MpBES1 can behave as a gain-of-function substitute of *Arabidopsis* BEHs (Figures S4D and S4E).

In angiosperms, phosphorylation mediated by GLYCOGEN SYNTHASE KINASE 3 (GSK3) kinases determines key functional properties of BEH proteins, such as DNA binding, subcellular localization, and stability.[16,37] AtBZR1 and AtBES1 interact with BIN2 through a short C-terminal docking motif adjacent to the EAR domain;[21] this motif is absent in MpBES1 but is present in all angiosperm BEHs. We therefore assayed the ability of MpBES1 to interact with and be phosphorylated by GSK3s, in particular the sole GSK3 kinase in Marchantia (MpGSK) (Mp7g04170). In Y2H assays, AtBES1 readily interacted with both BIN2 and MpGSK, whereas MpBES1 interacted more weakly with BIN2 and not at all with MpGSK (Figure 4D). When transiently co-expressed in *Nicotiana benthamiana*, MpBES1 could be fully phosphorylated by BIN2 but only partially by MpGSK (Figure 4E), whereas both AtBES1 and AtBEH3 (an *Arabidopsis* BEH protein that lacks the 14-3-3 binding site and the

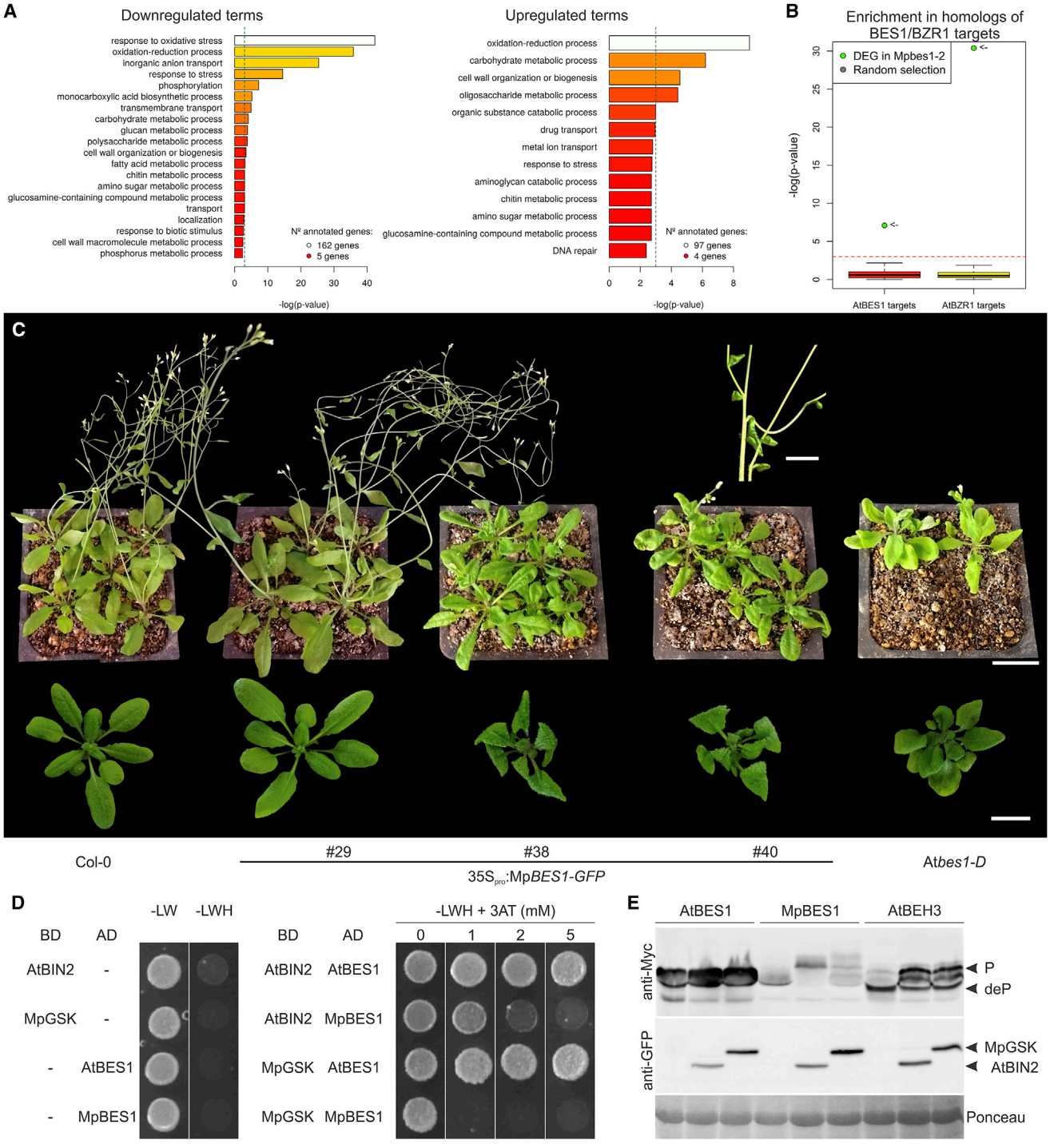

Figure 4. Similarities and differences between MpBES1 and AtBES1

(A) GO enrichment analysis of genes deregulated in Mp*bes1-2* plants. Left: among downregulated genes, oxidative processes, transport, and response to stress categories are over-represented. Right: among upregulated genes, oxidative processes, carbohydrate metabolism, and cell wall modification are over-represented. Bar length denotes the enrichment value (−log(p value)), whereas bar color denotes the number of deregulated genes annotated in each category. See Data S2 for the list of deregulated genes and enriched GO terms.

(B) *Arabidopsis* BES1 and BZR1 direct targets are over-represented among homologous Marchantia genes deregulated in the Mp*bes1-2* mutant. Green points denote the actual enrichment for homologs of AtBES1 and AtBZR1 targets among genes deregulated in the Mp*bes1-2* mutant, whereas boxplots denote p values for a 100-time bootstrapping, randomly selecting the same number of genes from the Marchantia genome. High (−log) p values suggest that MpBES1 regulates a similar set of homologous target genes as AtBES1 and AtBZR1.

(legend continued on next page)

PEST domain) reacted similarly with both kinases. Whereas the conserved N-terminal DBD and C-terminal EAR motif seem to warrant the basic functions of BEH proteins in all land plants, differences in the regulatory C-terminal domain may allow MpBES1 to evade the control mechanisms acting on its *Arabidopsis* homologs. Remarkably, MpBES1 is able to respond to BRs *in vivo* in *Arabidopsis*, as shown by a change in the electrophoretic mobility of the protein upon treatments with BL or LiCl, a general inhibitor of GSK3 (Figure S4F).

Concluding remarks

Our results uncover the crucial role of MpBES1 controlling cell proliferation and differentiation in Marchantia and hint to the possible ancestral functions of the BEH transcription factor family in the land-plant lineage. Liverworts lack BRL-type receptors but have identifiable homologs of the peptide-binding receptors PHLOEM INTERCALATED WITH XYLEM (PXY) (also known as TDIF RECEPTOR [TDR]; for instance, Mp1g09960) and EXCESS MICROSPOROCYTES 1 (EMS1) (Mp4g12310) that in *Arabidopsis* regulate, through BEHs, the differentiation of xylem and of tapetal cells in anthers, respectively.[38–40] However, we and others have recently shown that BRL genes are probably an ancestral feature of land plants that liverworts have secondarily dispensed with.[11,12] It will be worth exploring to what extent ancestral BEHs responded to peptide signals or to the thus-far-unknown signal/s originally perceived by BRLs.

Our results also point at common regulatory mechanisms operating on BEH proteins. The tight interaction between BEHs and GSK3s likely evolved after the split between bryophytes and tracheophytes, but the potential to become phosphorylated by GSK3s seems to be a theme of the family. Phosphorylation appears to be more a kinetic than a thermodynamic feature of BEHs, depending on the ability of the transcription factor and kinase to come into close contact with each other: in our experimental conditions, MpBES1 was as readily phosphorylated by BIN2 as its *Arabidopsis* homologs. The SAPVTP motif is a highly conserved feature of land-plant BEHs and bears the signature of GSK3 targets, i.e., a Ser/Thr separated by three residues from a Pro-associated Ser/Thr (S/TxxxS/TP). The N-terminal Ser in this motif is part of the 14-3-3 binding site responsible for the cytoplasmic retention of phosphorylated AtBES1/AtBZR1;[16,17] the absence of this site may increase the nuclear partitioning of MpBES1 and contribute to its gain-of-function behavior when expressed in *Arabidopsis*. It is still possible that, *in vivo*, MpBES1 is phosphorylated by MpGSK, provided both proteins are recruited in close proximity by a bridging partner. Not only did the affinity of BEHs toward GSK3 increase in angiosperms, but it is also plausible that GSK3s became more active toward BEHs. This effect is probably masked in AtBEH proteins because the presence of the GSK3-docking motif makes for a high-affinity, saturating interaction but becomes apparent in the differential activity of BIN2 and MpGSK toward MpBES1. These changes have probably contributed to more readily control the phosphorylation state of BEHs.

In both Mp*bes1* and Mp*tcp1* mutants, cell proliferation is altered and the "oxidation-reduction process" category is significantly enriched among deregulated genes.[26] Of note, the activity of both proteins is also redox sensitive.[15,41] In angiosperms, local high concentrations of H_2O_2 maintain quiescence in dormant buds, whereas outgrowth activation correlates with the induction of peroxide-processing enzymes.[42] Likewise, the quiescent center (QC) in roots resides in an oxidative niche associated with a local auxin maximum; perturbations in the auxin flow that lead to a more reducing environment trigger cell divisions in the QC.[43] QC cells can also be forced to divide with BL treatments or through the expression of the overactive At*BES1-D* protein.[44] Even though extant Zygnematales are unicellular or filamentous organisms, the transition from proliferative to quiescent life stages or the production of differentiated structures like gametes or pre-akinetes possibly involves local redox changes with impact on the oxidation state of key transcriptional regulators.[45] It is conceivable that ancestral BEH proteins may have modulated the exit rate from indeterminate groups of cells in response to endogenous or environmental inputs, linking redox homeostasis to cell cycle progression and differentiation in stem cell niches.

The analysis of master regulator genes that shared a common ancestor over 450 mya sets a framework to understand the evolutionary processes that shaped BR signaling. Similar to the way ancestral auxin response factors became responsive to auxin in land plants,[46,47] an ancient transcriptional module controlling cell proliferation and differentiation was co-opted by BR perception; new regulatory layers paved the way to an increasingly fine-tuned growth control.

STAR★METHODS

Detailed methods are provided in the online version of this paper and include the following:

- KEY RESOURCES TABLE
- RESOURCE AVAILABILITY
  - Lead contact
  - Materials availability
  - Data and code availability
- EXPERIMENTAL MODEL AND SUBJECT DETAILS
  - Plant Materials and Growth Conditions
- METHOD DETAILS

(C) *Arabidopsis* plants overexpressing Mp*BES1* display a phenotypic syndrome similar to that of *bes1-D* gain-of-function mutants. Phenotype of 3-week-old (lower tier, scale bar, 1 cm) and 6-week-old (upper tier, scale bar, 2 cm) *Arabidopsis* plants of the indicated genotypes is shown (WT, three independent transgenic lines, and At*bes1-D*, all in Col-0 background). Inset: detail of the inflorescence of a 9-week-old $35S_{pro}$:Mp*BES1*-GFP no. 40 plant is shown; bends are due to the partial fusion between stem and cauline leaves; scale bars, 2 cm. See also Figure S4A for MpBES1 protein accumulation in these lines and Figure S4C for phenotypic comparisons.

(D) AtBES1 and MpBES1 display differential interactions with the GSK3 kinases AtBIN2/AtSK21 and MpGSK. *S. cerevisiae* AH109 carrying the indicated combinations of plasmids were spotted on selective medium lacking Leu, Trp, and His and the indicated amounts of 3AT.

(E) The ability of GSK3 kinases to phosphorylate BEHs depends on both the substrate and the kinase. myc-tagged BEHs and GFP-tagged GSK3 kinases were transiently expressed for 60 h in *N. benthamiana* leaves and detected with the corresponding antibodies. BEH phosphorylated forms have slower electrophoretic mobility, as indicated.

- Phylogenetic analysis
- Cloning and plasmid construction for plant transformation
- Transformation of Marchantia polymorpha
- Transformation of *Arabidopsis*
- Protein detection
- Microscopy and histochemical assays
- Quantitative real-time PCR (qRT-PCR)
- RNA sequencing and analysis
- Dual luciferase transactivation assay for BR binding elements
- Yeast one-hybrid assay
- Yeast two-hybrid assay
- Phosphorylation of BEH proteins
- Brassinazole treatment
- eBL and LiCl treatments

● QUANTIFICATION AND STATISTICAL ANALYSIS

- General statistical analyses
- RNA sequencing data analyses
- Search for enrichment in *cis*-regulatory elements

SUPPLEMENTAL INFORMATION

Supplemental information can be found online at https://doi.org/10.1016/j.cub.2021.08.050.

ACKNOWLEDGMENTS

We thank T. Kohchi for providing CRISPR and pMpGWB308 vectors, J. Bowman for amiR vectors, U. Lagercratz for the MpPRR:LUC line, M.A. Blázquez for the BRBE+ and BRBE− plasmids, Y. Yin for the anti-AtBES1 antibody, and Sequentia Biotec for support with RNA-seq. We acknowledge R. Solano and I. Monte for their help to initiate work on Marchantia and L. Civera for technical assistance in generating transgenics. M.A.M. and F.L.-E. received funding from FEDER-BIO2016-78150-P and PIRSES-GA-2013-612583. M.G.-H. is supported by the National Agency for the Promotion of Science and Technology (ANPCyT, Argentina). M.M.-B., D.B.-E., and F.L.-E. are funded by ERC-2015-CoG–683163 granted to A.I.C.-D. A.P.-R. is recipient of a PhD fellowship from the "Severo Ochoa Programme for Centers of Excellence in R&D" 2016–2019 from the Ministerio de Ciencia e Innovación, Spain (SEV-2015-0533). We acknowledge financial support from the Spanish Ministry of Science and Innovation-State Research Agency (AEI), through the "Severo Ochoa Programme for Centres of Excellence in R&D" SEV-2015-0533 and CEX2019-000902-S, and support from the CERCA Programme/Generalitat de Catalunya. S.M.-G. is a member of the National Research Council of Science and Technology (CONICET, Argentina); work in his laboratory was supported by a grant from ANPCyT (PICT2016-2234). A.I.C.-D. has received funding from the European Research Council (ERC) under the European Union's Horizon 2020 research and innovation programme (grant agreement no. 683163). The funders had no role in study design, data collection and analysis, decision to publish, or preparation of the manuscript.

AUTHOR CONTRIBUTIONS

Conceptualization, M.A.M., S.M.-G., and A.I.C.-D.; formal analysis, M.A.M., M.G.-H., F.L.-E., A.P.-R., M.M.-B., D.B.-E., S.M.-G., and A.I.C.-D.; investigation, M.A.M., M.G.-H., A.P.-R., M.M.-B., and D.B.-E.; methodology, M.A.M. and M.G.-H.; validation, M.A.M., M.G.-H., F.L.-E., A.P.-R., M.M.-B., D.B.-E., S.M.-G., and A.I.C.-D.; visualization, M.A.M., M.G.-H., F.L.-E., A.P.-R., M.M.-B., and D.B.-E.; writing – original draft, M.A.M., S.M.-G., and A.I.C.-D.; writing – review & editing, M.A.M., M.G.-H., F.L.-E., A.P.-R., M.M.-B., D.B.-E., S.M.-G., and A.I.C.-D.; data curation, M.G.-H. and F.L.-E.; software, M.G.-H. and F.L.-E.; funding acquisition, S.M.-G. and A.I.C.-D.; project administration, S.M.-G. and A.I.C.-D.; supervision, S.M.-G. and A.I.C.-D.

DECLARATION OF INTERESTS

The authors declare no competing interests.

INCLUSION AND DIVERSITY

One or more of the authors of this paper self-identifies as a member of the LGBTQ+ community. While citing references scientifically relevant for this work, we also actively worked to promote gender balance in our reference list.

Received: February 19, 2021
Revised: May 24, 2021
Accepted: August 18, 2021
Published: September 15, 2021

REFERENCES

1. Planas-Riverola, A., Gupta, A., Betegón-Putze, I., Bosch, N., Ibañes, M., and Caño-Delgado, A.I. (2019). Brassinosteroid signaling in plant development and adaptation to stress. Development *146*, dev151894.
2. González-García, M.-P., Vilarrasa-Blasi, J., Zhiponova, M., Divol, F., Mora-García, S., Russinova, E., and Caño-Delgado, A.I. (2011). Brassinosteroids control meristem size by promoting cell cycle progression in Arabidopsis roots. Development *138*, 849–859.
3. Hacham, Y., Holland, N., Butterfield, C., Ubeda-Tomas, S., Bennett, M.J., Chory, J., and Savaldi-Goldstein, S. (2011). Brassinosteroid perception in the epidermis controls root meristem size. Development *138*, 839–848.
4. Bell, E.M., Lin, W.C., Husbands, A.Y., Yu, L., Jaganatha, V., Jablonska, B., Mangeon, A., Neff, M.M., Girke, T., and Springer, P.S. (2012). Arabidopsis lateral organ boundaries negatively regulates brassinosteroid accumulation to limit growth in organ boundaries. Proc. Natl. Acad. Sci. USA *109*, 21146–21151.
5. Gendron, J.M., Liu, J.-S., Fan, M., Bai, M.-Y., Wenkel, S., Springer, P.S., Barton, M.K., and Wang, Z.-Y. (2012). Brassinosteroids regulate organ boundary formation in the shoot apical meristem of Arabidopsis. Proc. Natl. Acad. Sci. USA *109*, 21152–21157.
6. Yang, J., Thames, S., Best, N.B., Jiang, H., Huang, P., Dilkes, B.P., and Eveland, A.L. (2018). Brassinosteroids modulate meristem fate and differentiation of unique inflorescence morphology in *Setaria viridis*. Plant Cell *30*, 48–66.
7. Belkhadir, Y., and Jaillais, Y. (2015). The molecular circuitry of brassinosteroid signaling. New Phytol. *206*, 522–540.
8. Yin, Y., Wang, Z.Y., Mora-Garcia, S., Li, J., Yoshida, S., Asami, T., and Chory, J. (2002). BES1 accumulates in the nucleus in response to brassinosteroids to regulate gene expression and promote stem elongation. Cell *109*, 181–191.
9. Wang, Z.Y., Nakano, T., Gendron, J., He, J., Chen, M., Vafeados, D., Yang, Y., Fujioka, S., Yoshida, S., Asami, T., and Chory, J. (2002). Nuclear-localized BZR1 mediates brassinosteroid-induced growth and feedback suppression of brassinosteroid biosynthesis. Dev. Cell *2*, 505–513.
10. Yokota, T., Ohnishi, T., Shibata, K., Asahina, M., Nomura, T., Fujita, T., Ishizaki, K., and Kohchi, T. (2017). Occurrence of brassinosteroids in non-flowering land plants, liverwort, moss, lycophyte and fern. Phytochemistry *136*, 46–55.
11. Ferreira-Guerra, M., Marquès-Bueno, M., Mora-García, S., and Caño-Delgado, A.I. (2020). Delving into the evolutionary origin of steroid sensing in plants. Curr. Opin. Plant Biol. *57*, 87–95.
12. Furumizu, C., and Sawa, S. (2021). Insight into early diversification of leucine-rich repeat receptor-like kinases provided by the sequenced moss and hornwort genomes. Plant Mol. Biol. Published online January 3, 2021. https://doi.org/10.1007/s11103-020-01100-0.
13. Nosaki, S., Miyakawa, T., Xu, Y., Nakamura, A., Hirabayashi, K., Asami, T., Nakano, T., and Tanokura, M. (2018). Structural basis for brassinosteroid response by BIL1/BZR1. Nat. Plants *4*, 771–776.

14. Reinhold, H., Soyk, S., Simková, K., Hostettler, C., Marafino, J., Mainiero, S., Vaughan, C.K., Monroe, J.D., and Zeeman, S.C. (2011). β-amylase-like proteins function as transcription factors in Arabidopsis, controlling shoot growth and development. Plant Cell *23*, 1391–1403.

15. Tian, Y., Fan, M., Qin, Z., Lv, H., Wang, M., Zhang, Z., Zhou, W., Zhao, N., Li, X., Han, C., et al. (2018). Hydrogen peroxide positively regulates brassinosteroid signaling through oxidation of the BRASSINAZOLE-RESISTANT1 transcription factor. Nat. Commun. *9*, 1063.

16. Gampala, S.S., Kim, T.-W., He, J.-X., Tang, W., Deng, Z., Bai, M.-Y., Guan, S., Lalonde, S., Sun, Y., Gendron, J.M., et al. (2007). An essential role for 14-3-3 proteins in brassinosteroid signal transduction in Arabidopsis. Dev. Cell *13*, 177–189.

17. Ryu, H., Kim, K., Cho, H., Park, J., Choe, S., and Hwang, I. (2007). Nucleocytoplasmic shuttling of BZR1 mediated by phosphorylation is essential in Arabidopsis brassinosteroid signaling. Plant Cell *19*, 2749–2762.

18. Oh, E., Zhu, J.-Y., Ryu, H., Hwang, I., and Wang, Z.-Y. (2014). TOPLESS mediates brassinosteroid-induced transcriptional repression through interaction with BZR1. Nat. Commun. *5*, 4140.

19. Espinosa-Ruiz, A., Martínez, C., de Lucas, M., Fàbregas, N., Bosch, N., Caño-Delgado, A.I., and Prat, S. (2017). TOPLESS mediates brassinosteroid control of shoot boundaries and root meristem development in *Arabidopsis thaliana*. Development *144*, 1619–1628.

20. Tang, W., Yuan, M., Wang, R., Yang, Y., Wang, C., Oses-Prieto, J.A., Kim, T.-W., Zhou, H.-W., Deng, Z., Gampala, S.S., et al. (2011). PP2A activates brassinosteroid-responsive gene expression and plant growth by dephosphorylating BZR1. Nat. Cell Biol. *13*, 124–131.

21. Peng, P., Zhao, J., Zhu, Y., Asami, T., and Li, J. (2010). A direct docking mechanism for a plant GSK3-like kinase to phosphorylate its substrates. J. Biol. Chem. *285*, 24646–24653.

22. Solly, J.E., Cunniffe, N.J., and Harrison, C.J. (2017). Regional growth rate differences specified by apical notch activities regulate liverwort thallus shape. Curr. Biol. *27*, 16–26.

23. Hisanaga, T., Kawade, K., and Tsukaya, H. (2015). Compensation: a key to clarifying the organ-level regulation of lateral organ size in plants. J. Exp. Bot. *66*, 1055–1063.

24. Suzuki, H., Harrison, C.J., Shimamura, M., Kohchi, T., and Nishihama, R. (2020). Positional cues regulate dorsal organ formation in the liverwort Marchantia polymorpha. J. Plant Res. *133*, 311–321.

25. Linde, A.-M., Eklund, D.M., Kubota, A., Pederson, E.R.A., Holm, K., Gyllenstrand, N., Nishihama, R., Cronberg, N., Muranaka, T., Oyama, T., et al. (2017). Early evolution of the land plant circadian clock. New Phytol. *216*, 576–590.

26. Busch, A., Deckena, M., Almeida-Trapp, M., Kopischke, S., Kock, C., Schüssler, E., Tsiantis, M., Mithöfer, A., and Zachgo, S. (2019). MpTCP1 controls cell proliferation and redox processes in Marchantia polymorpha. New Phytol. *224*, 1627–1641.

27. Müssig, C., Lisso, J., Coll-Garcia, D., and Altmann, T. (2006). Molecular analysis of brassinosteroid action. Plant Biol. *8*, 291–296.

28. Sun, Y., Fan, X.-Y., Cao, D.-M., Tang, W., He, K., Zhu, J.-Y., He, J.-X., Bai, M.-Y., Zhu, S., Oh, E., et al. (2010). Integration of brassinosteroid signal transduction with the transcription network for plant growth regulation in Arabidopsis. Dev. Cell *19*, 765–777.

29. Yu, X., Li, L., Zola, J., Aluru, M., Ye, H., Foudree, A., Guo, H., Anderson, S., Aluru, S., Liu, P., et al. (2011). A brassinosteroid transcriptional network revealed by genome-wide identification of BESI target genes in Arabidopsis thaliana. Plant J. *65*, 634–646.

30. Zhiponova, M.K., Vanhoutte, I., Boudolf, V., Betti, C., Dhondt, S., Coppens, F., Mylle, E., Maes, S., González-García, M.-P., Caño-Delgado, A.I., et al. (2013). Brassinosteroid production and signaling differentially control cell division and expansion in the leaf. New Phytol. *197*, 490–502.

31. Cheng, P., Liu, Y., Yang, Y., Chen, H., Cheng, H., Hu, Q., Zhang, Z., Gao, J., Zhang, J., Ding, L., et al. (2020). *CmBES1* is a regulator of boundary formation in chrysanthemum ray florets. Hortic. Res. *7*, 129.

32. Sun, S., Chen, D., Li, X., Qiao, S., Shi, C., Li, C., Shen, H., and Wang, X. (2015). Brassinosteroid signaling regulates leaf erectness in Oryza sativa via the control of a specific U-type cyclin and cell proliferation. Dev. Cell *34*, 220–228.

33. Hu, Y., Bao, F., and Li, J. (2000). Promotive effect of brassinosteroids on cell division involves a distinct CycD3-induction pathway in Arabidopsis. Plant J. *24*, 693–701.

34. He, J.-X., Gendron, J.M., Sun, Y., Gampala, S.S.L., Gendron, N., Sun, C.Q., and Wang, Z.-Y. (2005). BZR1 is a transcriptional repressor with dual roles in brassinosteroid homeostasis and growth responses. Science *307*, 1634–1638.

35. Gallego-Bartolomé, J., Minguet, E.G., Grau-Enguix, F., Abbas, M., Locascio, A., Thomas, S.G., Alabadí, D., and Blázquez, M.A. (2012). Molecular mechanism for the interaction between gibberellin and brassinosteroid signaling pathways in Arabidopsis. Proc. Natl. Acad. Sci. USA *109*, 13446–13451.

36. Kim, H., Shim, D., Moon, S., Lee, J., Bae, W., Choi, H., Kim, K., and Ryu, H. (2019). Transcriptional network regulation of the brassinosteroid signaling pathway by the BES1-TPL-HDA19 co-repressor complex. Planta *250*, 1371–1377.

37. Vert, G., and Chory, J. (2006). Downstream nuclear events in brassinosteroid signalling. Nature *441*, 96–100.

38. Kondo, Y., Ito, T., Nakagami, H., Hirakawa, Y., Saito, M., Tamaki, T., Shirasu, K., and Fukuda, H. (2014). Plant GSK3 proteins regulate xylem cell differentiation downstream of TDIF-TDR signalling. Nat. Commun. *5*, 3504.

39. Zheng, B., Bai, Q., Wu, L., Liu, H., Liu, Y., Xu, W., Li, G., Ren, H., She, X., and Wu, G. (2019). EMS1 and BRI1 control separate biological processes via extracellular domain diversity and intracellular domain conservation. Nat. Commun. *10*, 4165.

40. Chen, W., Lv, M., Wang, Y., Wang, P.-A., Cui, Y., Li, M., Wang, R., Gou, X., and Li, J. (2019). BES1 is activated by EMS1-TPD1-SERK1/2-mediated signaling to control tapetum development in Arabidopsis thaliana. Nat. Commun. *10*, 4164.

41. Viola, I.L., Güttlein, L.N., and Gonzalez, D.H. (2013). Redox modulation of plant developmental regulators from the class I TCP transcription factor family. Plant Physiol. *162*, 1434–1447.

42. Porcher, A., Guérin, V., Montrichard, F., Lebrec, A., Lothier, J., and Vian, A. (2020). Ascorbate glutathione-dependent H2O2 scavenging is an important process in axillary bud outgrowth in rosebush. Ann. Bot. *126*, 1049–1062.

43. Yu, Q., Tian, H., Yue, K., Liu, J., Zhang, B., Li, X., and Ding, Z. (2016). A P-loop NTPase regulates quiescent center cell division and distal stem cell identity through the regulation of ROS homeostasis in Arabidopsis root. PLoS Genet. *12*, e1006175.

44. Lozano-Elena, F., Planas-Riverola, A., Vilarrasa-Blasi, J., Schwab, R., and Caño-Delgado, A.I. (2018). Paracrine brassinosteroid signaling at the stem cell niche controls cellular regeneration. J. Cell Sci. *131*, jcs204065.

45. Holzinger, A., and Pichrtová, M. (2016). Abiotic stress tolerance of charophyte green algae: new challenges for omics techniques. Front. Plant Sci. *7*, 678.

46. Martin-Arevalillo, R., Thévenon, E., Jégu, F., Vinos-Poyo, T., Vernoux, T., Parcy, F., and Dumas, R. (2019). Evolution of the auxin response factors from charophyte ancestors. PLoS Genet. *15*, e1008400.

47. Mutte, S.K., Kato, H., Rothfels, C., Melkonian, M., Wong, G.K.-S., and Weijers, D. (2018). Origin and evolution of the nuclear auxin response system. eLife *7*, e33399.

48. Koncz, C., and Schell, J. (1986). The promoter of T_L-DNA gene *5* controls the tissue-specific expression of chimaeric genes carried by a novel type of *Agrobacterium* binary vector. Mol. Gen. Genet. *204*, 383–396.

49. Gamborg, O.L., Miller, R.A., and Ojima, K. (1968). Nutrient requirements of suspension cultures of soybean root cells. Exp. Cell Res. *50*, 151–158.

50. Xu, W., Huang, J., Li, B., Li, J., and Wang, Y. (2008). Is kinase activity essential for biological functions of BRI1? Cell Res. *18*, 472–478.

51. Ishizaki, K., Chiyoda, S., Yamato, K.T., and Kohchi, T. (2008). Agrobacterium-mediated transformation of the haploid liverwort Marchantia polymorpha L., an emerging model for plant biology. Plant Cell Physiol. *49*, 1084–1091.

52. Sugano, S.S., Nishihama, R., Shirakawa, M., Takagi, J., Matsuda, Y., Ishida, S., Shimada, T., Hara-Nishimura, I., Osakabe, K., and Kohchi, T. (2018). Efficient CRISPR/Cas9-based genome editing and its application to conditional genetic analysis in Marchantia polymorpha. PLoS ONE *13*, e0205117.

53. Flores-Sandoval, E., Eklund, D.M., Hong, S.F., Alvarez, J.P., Fisher, T.J., Lampugnani, E.R., et al. (2018). Class C ARFs evolved before the origin of land plants and antagonize differentiation and developmental transitions in *Marchantia polymorpha*. New Phytol. *218*, 1612–1630.

54. Flores-Sandoval, E., Dierschke, T., Fisher, T.J., and Bowman, J.L. (2016). Efficient and inducible use of artificial microRNAs in Marchantia polymorpha. Plant Cell Physiol. *57*, 281–290.

55. Ishizaki, K., Nishihama, R., Ueda, M., Inoue, K., Ishida, S., Nishimura, Y., Shikanai, T., and Kohchi, T. (2015). Development of gateway binary vector series with four different selection markers for the liverwort Marchantia polymorpha. PLoS ONE *10*, e0138876.

56. Earley, K.W., Haag, J.R., Pontes, O., Opper, K., Juehne, T., Song, K., and Pikaard, C.S. (2006). Gateway-compatible vectors for plant functional genomics and proteomics. Plant J. *45*, 616–629.

57. Castrillo, G., Turck, F., Leveugle, M., Lecharny, A., Carbonero, P., Coupland, G., Paz-Ares, J., and Oñate-Sánchez, L. (2011). Speeding cis-trans regulation discovery by phylogenomic analyses coupled with screenings of an arrayed library of Arabidopsis transcription factors. PLoS ONE *6*, e21524.

58. Rossignol, P., Collier, S., Bush, M., Shaw, P., and Doonan, J.H. (2007). Arabidopsis POT1A interacts with TERT-V(I8), an N-terminal splicing variant of telomerase. J. Cell Sci. *120*, 3678–3687.

59. Karimi, M., Inzé, D., and Depicker, A. (2002). GATEWAY vectors for Agrobacterium-mediated plant transformation. Trends Plant Sci. *7*, 193–195.

60. Kumar, S., Stecher, G., Li, M., Knyaz, C., and Tamura, K. (2018). MEGA X: molecular evolutionary genetics analysis across computing platforms. Mol. Biol. Evol. *35*, 1547–1549.

61. Larkin, M.A., Blackshields, G., Brown, N.P., Chenna, R., McGettigan, P.A., McWilliam, H., et al. (2007). Clustal W and Clustal X version 2.0. Bioinformatics *23*, 2947–2948.

62. Schneider, C.A., Rasband, W.S., and Eliceiri, K.W. (2012). NIH Image to ImageJ: 25 years of image analysis. Nat. Methods *9*, 671–675.

63. Bushnell, B. (2014). BBMap: a fast, accurate, splice-aware aligner. https://www.osti.gov/servlets/purl/1241166.

64. Dobin, A., Davis, C.A., Schlesinger, F., Drenkow, J., Zaleski, C., Jha, S., Batut, P., Chaisson, M., and Gingeras, T.R. (2013). STAR: ultrafast universal RNA-seq aligner. Bioinformatics *29*, 15–21.

65. Liao, Y., Smyth, G.K., and Shi, W. (2014). featureCounts: an efficient general purpose program for assigning sequence reads to genomic features. Bioinformatics *30*, 923–930.

66. R Development Core Team (2020). R: A language and environment for statistical computing (R Foundation for Statistical Computing).

67. Rau, A., Gallopin, M., Celeux, G., and Jaffrézic, F. (2013). Data-based filtering for replicated high-throughput transcriptome sequencing experiments. Bioinformatics *29*, 2146–2152.

68. McCarthy, D.J., Chen, Y., and Smyth, G.K. (2012). Differential expression analysis of multifactor RNA-Seq experiments with respect to biological variation. Nucleic Acids Res. *40*, 4288–4297.

69. Alexa, A., Rahnenfuhrer, J. (2021). topGO: enrichment analysis for gene ontology. R package version 2.44.0.

70. Heinz, S., Benner, C., Spann, N., Bertolino, E., Lin, Y.C., Laslo, P., Cheng, J.X., Murre, C., Singh, H., and Glass, C.K. (2010). Simple combinations of lineage-determining transcription factors prime cis-regulatory elements required for macrophage and B cell identities. Mol. Cell *38*, 576–589.

71. Flores-Sandoval, E., Romani, F., and Bowman, J.L. (2018). Co-expression and transcriptome analysis of *Marchantia polymorpha* transcription factors supports class C ARFs as independent actors of an ancient auxin regulatory module. Front. Plant Sci. *9*, 1345.

72. Kubota, A., Ishizaki, K., Hosaka, M., and Kohchi, T. (2013). Efficient Agrobacterium-mediated transformation of the liverwort Marchantia polymorpha using regenerating thalli. Biosci. Biotechnol. Biochem. *77*, 167–172.

73. Clough, S.J., and Bent, A.F. (1998). Floral dip: a simplified method for Agrobacterium-mediated transformation of Arabidopsis thaliana. Plant J. *16*, 735–743.

74. Livak, K.J., and Schmittgen, T.D. (2001). Analysis of relative gene expression data using real-time quantitative PCR and the 2(-Δ Δ C(T)) method. Methods *25*, 402–408.

75. Saint-Marcoux, D., Proust, H., Dolan, L., and Langdale, J.A. (2015). Identification of reference genes for real-time quantitative PCR experiments in the liverwort Marchantia polymorpha. PLoS ONE *10*, e0118678.

76. Gietz, R.D., and Woods, R.A. (2002). Transformation of yeast by lithium acetate/single-stranded carrier DNA/polyethylene glycol method. Methods Enzymol. *350*, 87–96.

STAR★METHODS

KEY RESOURCES TABLE

REAGENT or RESOURCE	SOURCE	IDENTIFIER
Antibodies		
Anti-GFP	Thermo Fisher Scientific	Cat#A6455; RRID: AB_221570
Anti-GFP	Labome	Cat#TP401; RRID: AB_10013661
Anti-myc	Sigma-Aldrich	Cat#SAB1305535
Anti-AtBES1	Yin et al.[8]	N/A
Anti-Rabbit IgG (whole molecule), F(ab')2 fragment–Peroxidase antibody produced in goat	Sigma-Aldrich	Cat#A6667; RRID: AB_2863533
Anti-Mouse IgG (whole molecule)-Peroxidase antibody produced in rabbit	Sigma-Aldrich	Cat#A9044; RRID: AB_258431
Bacterial and virus strains		
Escherichia coli DH5α	Widely distributed	N/A
Agrobacterium tumefaciens GV3101	Koncz et al.[48]	N/A
Chemicals, peptides, and recombinant proteins		
Gamborg's B5 salts	Gamborg et al.[49]	N/A
Phyto Agar	Duchefa	Cat#P1003
Chlorsulfuron (Glean XP)	Dupont	EPA#352-653
Hygromycin B	Thermo Fisher Scientific	Cat#10687-010
Cefotaxime sodium	Duchefa	Cat#64485-93-4
3,5-Dimethoxy-4-hydroxyacetophenone (Acetosyringone)	Sigma-Aldrich	Cat#D134406
β-Estradiol	Sigma-Aldrich	Cat#E8875
3-Amino-1,2,4-triazole	Sigma-Aldrich	Cat#A8056
cOmplete Protease Inhibitor Cocktail	Sigma-Aldrich	Cat#04693116001
PhosSTOP	Sigma-Aldrich	Cat#4906845001
Basta 14SL	BASF	N/A
Phosphinothricin	Duchefa	Cat#P0159
D-Luciferin	Thermo Fisher Scientific	Cat#L2911
Yeast Nitrogen Base	Thermo Fisher Scientific	Cat#Q30007
Dropout supplement –Leu/–Trp	TakaraBio	Cat#630417
Dropout supplement –His/–Leu/–Trp	TakaraBio	Cat#630419
Murashige Skoog medium	Duchefa	Cat#M0221
24-Epi-Brassinolide	Sigma-Aldrich	Cat#B1439
Brassinazole	Sigma-Aldrich	Cat#SML1406
LiCl	Sigma-Aldrich	Cat#203637
Critical commercial assays		
Q5 High-Fidelity DNA Polymerase	New England Biolabs	Cat#M0491L
BsaI	New England Biolabs	Cat#R0535L
XbaI	New England Biolabs	Cat#R0145S
SacI	New England Biolabs	Cat#R0156S
KpnI	New England Biolabs	Cat#R3142S
HindIII	New England Biolabs	Cat#R3104S
NotI	New England Biolabs	Cat#R3189S
ScaI	New England Biolabs	Cat#R3122S
T4 DNA Ligase	Promega	Cat#M180A

(*Continued on next page*)

Continued

REAGENT or RESOURCE	SOURCE	IDENTIFIER
Gateway BP Clonase II Enzyme mix	Thermo Fisher Scientific	Cat#11789-020
Gateway LR Clonase II Enzyme mix	Thermo Fisher Scientific	Cat#11791-020
Novex ECL Chemiluminescent Substrate Reagent Kit	Thermo Fisher Scientific	Cat#WP20005
Technovit 7100 Embedding Kit	Energy Beam Sciences	Cat#64709003
Click-iT EdU (5-ethynyl-2′-deoxyuridine) Alexa Fluor 488 Imaging Kit	Thermo Fisher Scientific	Cat#C10329
Dual-Glo Luciferase Assay System	Promega	Cat#E1910
RNeasy Plant Mini Kit	QIAGEN	Cat#74904
TURBO DNAfreeTM Kit	Thermo Fisher Scientific	Cat#AM1907
SuperScript II Reverse Transcriptase	Thermo Fisher Scientific	Cat#18064022
SsoAdvanced Universal SYBR Green Supermix	BioRad	Cat#172-5270
Technovit 7100 Combipack	Kulzer Technique	Cat#64709003
TruSeq Stranded mRNA Sample Prep Kit	Illumina	Cat#20020594
TRIzol Reagent	Invitrogen	Cat#15596018
Agencourt AMPure Xp	Beckman Coulter	Cat#A63880
Deposited data		
Mp*BES1-2* RNA-seq data	This paper	GEO: GSE166913
Experimental models: organisms/strains		
Saccharomyces cerevisiae Y187	TakaraBio	Cat#630489
Saccharomyces cerevisiae Y2HGold	TakaraBio	Cat#630489
Nicotiana benthamiana lab strain	Widely distributed	N/A
Arabidopsis thaliana Columbia-0	Widely distributed	N/A
Arabidopsis thaliana bri1-301	[50]	N/A
Marchantia polymorpha: Tak-1	[51]	N/A
Marchantia polymorpha: Tak-1 Mp*bes1* (pMpGE010 Mp*BES1*-gRNA)	This paper	N/A
Marchantia polymorpha: Tak-1 ami*R*-Mp*BES1* (pHART01 Mp*EF1*α_{pro}:ami*R*-Mp*BES1*)	This paper	N/A
Marchantia polymorpha: Tak-1 ami*R*-Mp*BES1*^{ind} (pHART01 *lexA*$_{pro}$:ami*R*-Mp*BES1; MpEF1*α_{pro}*:XVE*)	This paper	N/A
Marchantia polymorpha: Tak-1 Mp*EF1*α_{pro}:Mp*BES1-Citrine* (pMpGWB308)	This paper	N/A
Marchantia polymorpha: MpPRR$_{pro}$*:LUC* (pMpGWB431)	[25]	N/A
Marchantia polymorpha: MpPRR$_{pro}$*:LUC* (pMpGWB431) *Mpbes1* (pMpGE010 Mp*BES1*-gRNA)	This paper	N/A
Arabidopsis thaliana: Col-0 35S$_{pro}$:Mp*BES1-GFP*	This paper	N/A
Arabidopsis thaliana: bri1-301 35S$_{pro}$:At*BES1-GFP*	This paper	N/A
Arabidopsis thaliana: bri1-301 35S$_{pro}$:At*bes1-D-GFP*	This paper	N/A
Arabidopsis thaliana: At*bes1-D* (introgressed into Col-0 background)	[8]	N/A
Arabidopsis thaliana: At*bzr1-D*	[9]	N/A

(*Continued on next page*)

Continued		
REAGENT or RESOURCE	SOURCE	IDENTIFIER
Oligonucleotides		
See Table S1	This paper	N/A
Recombinant DNA		
35S$_{pro}$:P19	Widely distributed	N/A
pMpGE_En03	[52]	Addgene #71535
pMpGE_En03-Mp*BES1*-gRNA	This paper	N/A
pMpGE010	[52]	Addgene #71536
pMpGE010-Mp*BES1*-gRNA	This paper	N/A
pBJ36	[53]	N/A
pBJ36-Mp*EF1α$_{pro}$*:ami*R*-Mp*BES1*	This paper	N/A
pHART01	[53]	N/A
pHART01-Mp*EF1α$_{pro}$*:ami*R*-Mp*BES1*	This paper	N/A
pDONR201-ami*R*-Mp*BES1*	This paper	N/A
MpXVEindie	[54]	N/A
MpXVEindie *lexA$_{pro}$*:ami*R*-Mp*BES1*	This paper	N/A
pDONR221	Thermo Fisher Scientific	Cat#12536017
pDONR221-Mp*BES1*	This paper	N/A
pDONR221-At*BES1*	This paper	N/A
pDONR221-At*bes1-D*	This paper	N/A
pDONR221-At*BEH3*	This paper	N/A
pDONR221-Mp*GSK*	This paper	N/A
pDONR221-At*BIN2*	This paper	N/A
pDONR221-At*BZR1*	This paper	N/A
pMpGWB308	[55]	Addgene #68636
pMpGWB308-Mp*EF1α$_{pro}$*:Mp*BES1*	This paper	N/A
pEarleyGate103	[56]	N/A
pEarleyGate103-*35S$_{pro}$*:Mp*BES1*	This paper	N/A
pEarleyGate103-*35S$_{pro}$*:At*BES1*	This paper	N/A
pEarleyGate103-*35S$_{pro}$*:At*bes1-D*	This paper	N/A
pTUY1H	Castrillo et al.[57]	N/A
pTUY1H-At*CPD$_{pro}$*	This paper	N/A
pDEST22	Thermo Fisher Scientific	Cat#PQ10001-01
pDEST22-At*BES1*	This paper	N/A
pDEST22-At*BZR1*	This paper	N/A
pDEST22-Mp*BES1*	This paper	N/A
pGADT7-DEST	[58]	N/A
pGADT7-DEST-Mp*BES1*	This paper	N/A
pGADT7-DEST-At*BES1*	This paper	N/A
pGBKT7-DEST	[58]	N/A
pGBKT7-DEST-Mp*GSK*	This paper	N/A
pGBKT7-DEST-At*BIN2*	This paper	N/A
pEarleyGate203	[56]	N/A
pEarleyGate203-At*BES1*	This paper	N/A
pEarleyGate203-At*BZR1*	This paper	N/A
pEarleyGate203-At*BEH3*	This paper	N/A
pEarleyGate203-Mp*BES1*	This paper	N/A
pB7WGF2	Karimi et al.[59]	VIB-Ugent #1_42
pB7WGF2-At*BIN2*	This paper	N/A
pB7WGF2-Mp*GSK*	This paper	N/A
pGreenII 0800 CPD$_{pro}$x5:LUC (BRBE+)	Gallego-Bartolomé et al.[35]	N/A

(*Continued on next page*)

Continued

REAGENT or RESOURCE	SOURCE	IDENTIFIER
pGreenII 0800 CPD_{pro}x5mut:LUC (BRBE-)	Gallego Bartolomé et al.[35]	N/A
Software and algorithms		
MEGA X	Kumar et al.[60]	https://www.megasoftware.net/
ClustalW	[61]	http://www.clustal.org/
Prism8	GraphPad Software	https://www.graphpad.com:443/
ImageJ	Schneider et al.[62]	https://imagej.nih.gov/ij/
Imaris	Imaris Software	https://imaris.oxinst.com/
BBDuck	[63]	https://sourceforge.net/projects/bbmap/
STAR 2.5.2b	Dobin et al.[64]	https://github.com/alexdobin/STAR
FeatureCounts v1.5.1	Liao et al.[65]	http://subread.sourceforge.net/
R version 4.0.3	[66]	https://www.r-project.org/
R package HSTfilter	Rau et al. [67]	http://bioconductor.org/packages/release/bioc/html/HTSFilter.html
R package edgeR	McCarthy et al.[68]	http://bioconductor.org/packages/release/bioc/html/edgeR.html
R package TopGO	[69]	http://bioconductor.org/packages/release/bioc/html/topGO.html
Homer v4.11	Heinz et al.[70]	http://homer.ucsd.edu/homer/motif/
Other		
Data S1. WT and codon-optimized MpBES1 and ami*R*-Mp*BES1* sequences	This paper	N/A
Data S2. List of deregulated genes and enriched GO terms in the Mp*bes1-2* mutant	This paper	N/A

RESOURCE AVAILABILITY

Lead contact

Further information and requests for resources and reagents should be directed to and will be fulfilled by the Lead Contact Ana I. Caño-Delgado (ana.cano@cragenomica.es).

Materials availability

Plasmids and plant materials generated in this research are all available from the Leads Contacts upon request. Please note that the distribution of transgenic plants will be governed by material transfer agreements (MTAs) and will be dependent on appropriate import permits acquired by the receiver.

Data and code availability

Raw and processed RNA sequencing files have been deposited in the Gene Expression Omnibus (GEO) repository at the National Center for Biotechnology Information (NCBI) with the accession number GSE166913.

This paper does not report original code.

Any additional information required to reanalyze the data reported in this paper is available from the lead contact upon request.

EXPERIMENTAL MODEL AND SUBJECT DETAILS

Plant Materials and Growth Conditions

Marchantia polymorpha subsp. *ruderalis* cv. Tak1[51] was grown on half-strength Gamborg's B5 medium[49] adjusted at pH 5.7 and supplemented with 1% Phyto Agar (Duchefa), under white light (50 μmol photons/m^2/s) and long-day conditions (16 h light at 22°C, 8 h dark at 20°C, 60% relative humidity) either in walk-in growth chambers or in AL-30L2 growth chambers (Percival). To induce the production of sexual organs, plants were exposed to white light supplemented with far-red light (30 μmol photons/m^2/s).

Arabidopsis thaliana L. (Heyn) WT and *bri1-301*, *bzr1-D* and *bes1-D* mutants were in the Col-0 background. Seeds were surface sterilized with two washes of 70% Ethanol/0.02% Triton X-100 and two rinses with Ethanol 96%, spotted dried on sterile filter papers and placed on half-strength Murashige-Skoog (MS) medium (Duchefa) adjusted at pH 5.6 supplemented with 0.8% Phyto Agar (Duchefa). Seeds were stratified at 4°C for 48hs in the dark, and germinated under white light (80 μmol photons/m^2/s) and long-day

conditions (16 h light, 8 h dark at 22°C, 60% relative humidity) in AL-30L2 growth chambers (Percival). 10-day-old seedlings were transplanted into soil (1:1:1 v/v peat moss:vermiculite:perlite) and grown under a long-day photoperiod (16 hs light:8 hs dark, 23°C, 60% relative humidity) in walk-in growth chambers. *Nicotiana benthamiana* seeds were directly germinated in a 1:1:1 v/v peat moss:-vermiculite:perlite mix and grown under a long-day photoperiod (110 μmol photons/m^2/s, 16 hs light:8 hs dark, 23°C, 60% relative humidity) in walk-in growth chambers.

METHOD DETAILS

Phylogenetic analysis

Amino acid sequences in land plant and algae genomes were identified through TBLASTN searches. Sequences from *A.thaliana*, *Oryza sativa*, *Amborella trichopoda*, *Selaginella moellendorffii*, *Physcomitrella patens* and *M.polymorpha*, as representative species for angiosperms, lycophytes and bryophytes, respectively, were retrieved from Phytozome v13 (https://phytozome-next.jgi.doe.gov/). Sequences from the algae *Klebsormidium nitens* and *Mesotaenium endlicherianum* were retrieved from Phycocosm (https://phycocosm.jgi.doe.gov/phycocosm/home). Phylogenetic analysis was conducted in MEGA X.[60] Complete protein sequences were aligned using ClustalW and phylogenetic trees were constructed with the Maximum Likelihood method, using the Jones-Taylor-Thornton and G+I models and a bootstrap test of 1000 replicates.

Cloning and plasmid construction for plant transformation

MpBES1 guideRNA (gRNA)

CRISPR/Cas9-based genome editing of MpBES1 was performed as previously described.[52] Selection of the guideRNA (gRNA) target site was done using CasFinder (https://marchantia.info/tools/casfinder/) and the gRNA was designed in the DNA-binding domain (Figure S1C). Double stranded DNA (dsDNA) corresponding to the gRNA protospacers was generated by annealing complementary oligonucleotides and inserted into the pMpGE_En03 vector,[52] previously digested with BsaI, by ligation using DNA T4 ligase (Promega). Mp*BES1*-gRNA was incorporated into the binary vector pMpGE010[52] using Gateway LR Clonase II Enzyme mix (Thermo Fisher Scientific). Primers are included in Table S1.

amiR-MpBES1

a synthetic Mp*miR160* precursor encoding a 21-nt mature *amiR*-Mp*BES1* was synthesized by Genscript and designed to have KpnI/*Hind*III sites to subclone from puC57 into the shuttle plasmid pBJ36 downstream of Mp$EF1\alpha_{pro}$ by ligation, as previously described for the Mp*miR160* template.[71] Gel extraction of a band with a Mp$EF1\alpha_{pro}$:*amiR*-Mp*BES1* precursor by *Not*I/*Sca*I restriction which was inserted into pHART01 (Hyg^{Res}) expression vector by ligation.[71]

Inducible amiR-MpBES1

To create inducible constructs, the *amiR*-Mp*BES1* precursor with attachments was cloned into MpXVEindie vector via Gateway LR reaction (Thermo Fisher Scientific). MpXVEindie vector is an estrogen-inducible system with a pHART01 backbone downstream of a XVE-responsive promoter (*lexA*) and the XVE gene driven by the constitutive Mp$EF1\alpha_{pro}$.[54]

To generate pDONR201-Mp*BES1,* a version with reduced GC content compared to the native coding sequence was synthesized by Genscript with attB-containing primers and introduced into pDONR201 (Thermo Fisher Scientific) vector using Gateway BP Clonase II Enzyme mix (Thermo Fisher Scientific).

MpBES1 overexpression in Marchantia

The codon-optimized Mp*BES1* coding sequence (Data S1) was introduced intro the binary vector pMpGWB308[55] containing a MpEF1α promoter and a C-terminal in-frame Citrine sequence using Gateway LR Clonase II Enzyme mix (Thermo Fisher Scientific).

MpBES1, AtBES1 and Atbes1-D overexpression in Arabidopsis

The full length CDS of At*BES1* (At1g19350) and At*bes1-D* were amplified from cDNA by PCR using Q5 High-Fidelity DNA Polymerase (New England Biolabs) with attB-containing primers and introduced into pDONR201 (Thermo Fisher Scientific) vector using Gateway BP Clonase II Enzyme mix (Thermo Fisher Scientific). The codon-optimized Mp*BES1* (Data S1), At*BES1* and At*bes1-D* coding sequences were introduced into the binary vector pEarleyGate103[56] containing a *35S* promoter and a C-terminal in-frame GFP sequence using Gateway LR Clonase II Enzyme mix (Thermo Fisher Scientific).

All entry plasmids were confirmed by restriction enzyme digestion and Sanger sequencing. Destination vectors were confirmed by restriction enzyme digestion. Primers used are listed in Table S1.

Transformation of Marchantia polymorpha

Transformation of Marchantia was performed according to Kubota et al.[72] 15-day-old gemmalings grown as described were sliced to eliminate the apical notches and kept for 3 additional days in the same conditions on Gamborg's B5 medium supplemented with 1% sucrose. Regenerating thalli fragments were then co-incubated with *Agrobacterium tumefaciens* GV3101[48] cells carrying the corresponding vectors, resuspended at OD_{600nm}~0.02 in 0M51C medium (full strength Gamborg's B5 medium, 2% sucrose, 0.1% casamino acids, 0.03% L-glutamine) under white light and gentle shaking at 22°C. After three days, fragments were washed three times with sterile water and placed on Gamborg's B5 medium supplemented with 100 μg/ml cefotaxime (Duchefa) and either 10 μg/ml hygromicin B (Thermo Fisher Scientific) or 0.5 μM chlorosulfuron (Dupont). Transformation was carried out in Tak-1 and in the MpPRR_{pro}:*LUC* line[25] for the luciferase reporter assay. After 20 days, regenerating transgenic plants were transfered to fresh plates with the same additions. Given the strong growth disturbances caused by altered levels of MpBES1, transgenics plants were

propagated by vegetative cuttings. CRISPR-Cas9 mutation was assessed by PCR amplification of the target sequence followed by Sanger sequencing. Marchantia transgenic lines are listed in the Key resources table.

Transformation of *Arabidopsis*

pEarleyGate103:Mp*BES1*, pEarleyGate103:At*BES1* and pEarleyGate103:At*bes1-D* were transferred to *Agrobacterium tumefaciens* GV3101[48] and Col-0 plants were transformed by the flower dipping method.[73] T1 plants were selected on soil by spraying with a Basta solution; subsequent rounds of selection were performed on MS plates with the addition of 15 μg/ml phosphinothricin (Duchefa). For the selection of single-insertion lines, T2 seeds from individual T1 transgenic lines were plated regularly onto MS plates containing phosphinothricin, and the ratio of resistant to sensitive plants was scored 12 days later. Only lines that showed a ratio close to 3 resistant:1 sensitive were kept for further analysis, and transferred to soil. T3 seeds were scored under the same conditions to select homozygous, non-segregating lines for the transgenes. Selected lines were subsequently crossed with the *bri1-301* mutant.

Protein detection

50mg of tissue, either from thalli in Marchantia, young seedlings in *Arabidopsis* or portions of adult leaves in *N.benthamiana*, were collected, snap frozen in liquid N_2, ground to a fine powder in a mortar, and resuspended in 100ul of 100mM Tris-HCl (pH 6.8), 2% SDS, 200mM DTT, 7M urea with the addition of phosphatase (PhosSTOP) and protease (cOmplete) inhibitor cocktails (Sigma-Aldrich). Protein extracts were heated at 70°C for 10 minutes and loaded in 10% Tris-Glycine polyacrylamide gels. Proteins were separated by electrophoresis at 90V (constant voltage), transferred to PVDF membranes (BioRad) at 90V (constant voltage) and stained with Ponceau S. Membranes were blocked with 5% skimmed milk in TBS (50mM Tris-HCl pH 7.5/150mM NaCl) and revealed with the appropriate antibodies.

Microscopy and histochemical assays

Sectioning, staining and imaging

Resin embedding for semithin sectioning was performed with Technovit 7100 Combipack (Kulzer Technique) following manufacturer's instructions. Briefly, 30-day-old Marchantia plants were fixed in 1% (v/v) glutaraldehyde in 0.1 M sodium cacodylate buffer (pH 7.4). The samples were infiltrated under vacuum for 30 minutes and kept at 4°C for 24-72h. After fixation, samples were dehydrated through an 30%, 50%, 70%, 90%, and 100% (v/v) ethanol series for 60 minutes each. Historesin infiltration was started in a historesin-I:ethanol (1:1 v/v) solution for 1h and then the samples were incubated twice with 100% historesin-I for 60 min at room temperature and kept at 4°C overnight with fresh historesin-I. The samples were placed into molds and covered with historesin-II in anaerobic conditions for a week. The solidified blocks were cut in semithin sections (5-8 μm) using a glass knife in a RM2265 microtome (Leica). Transversal sections were stained with 0.1% (w/v) toluidine blue in 0.1M phosphate buffer (pH 7.2) for 10 s and rinsed with Milli-Q water. The samples were examined under a bright field DM6 microscope (Leica).

Scanning electron microscopy

Tissue samples were fixed using a 2.5% glutaraldehyde solution in 0.1M phosphate buffer (pH 7.4). After 24h the samples were post-fixed with 1% osmium tetroxide and then dehydrated through a graded ethanol series. Samples were dried using a critical point dryer (CPD030, Baltec) and sputter-coated with PdAu (Emitech). The samples were examined in a EVO MA10 microscope (Zeiss).

Confocal laser microscopy

Confocal laser scanning microscopy of Mp*EF1*α_{pro}:Mp*BES1-Citrine* thallus was performed using a FluoViewTM FV1000 microscope (Olympus), exciting with a 515 nm laser; chlorophyll was excited at 554 nm. Confocal laser scanning microscopy of *Arabidopsis 35S*$_{pro}$:Mp*BES1-GFP* seedlings was performed using a LSM510 Pascal microscope (Zeiss), exciting with a 488 nm laser.

Luciferase imaging

To visualize the expression pattern of luciferase in Mp*PRR*$_{pro}$*:LUC* and Mp*PRR*$_{pro}$*:LUC* Mp*bes1-7* lines, plants were sprayed with 1mM D-luciferin (Thermo Fisher Scientific). After 12 hours in continuous light, plants were placed in darkness and imaged with an ImageQuant Las-4000 CCD camera (GE HealthCare) for 10 minutes.

EdU staining

To assess the number of S-phase nuclei, we used the Click-iT EdU (5-ethynyl-2′-deoxyuridine) Alexa Fluor 488 Imaging Kit (Thermo Fisher Scientific). 3-day-old gemmalings of WT or an estradiol-inducible amiR-Mp*BES1* line, grown in Gamborg's B5 medium with and without 5μM β-estradiol (Sigma-Aldrich), were soaked in half-strength liquid medium with 10 μM EdU at 22°C for 2h under continuous white light. The samples were fixed in 50% (v/v) methanol/10% (v/v) acetic acid (fixative solution) at 4°C for at least 12h. After fixation, the samples were dehydrated through an ethanol series of 80%, 90% and 100% (v/v) and a final 90% (v/v) acetone incubation at 80°C for 5min each, followed by fixative solution at 22°C for 30min. The samples were washed four times with 0.5% (v/v) Triton X-100 in PBS (137 mM NaCl, 2.7 mM KCl, 10 mM Na_2HPO_4, 1.8 mM KH_2PO_4), incubated with the EdU detection cocktail following the manufacturer's instructions for 30 min in the dark with shaking at room temperature, and rinsed four times with 0.5% (v/v) Triton X-100 in PBS. Finally, the samples were transferred onto slides and incubated with chloral hydrate solution (25 g of chloral hydrate ($C_2H_3Cl_3O_2$) in 10 mL of H_2O) for 30min. Images were obtained using an FV1000 confocal microscope (Olympus). The number of dividing nuclei was quantified using the image analysis software Imaris (https://imaris.oxinst.com/). The number of meristems in the EdU-stained gemmalings was assessed by morphological observation and by the presence of stained nuclei.

Quantitative real-time PCR (qRT-PCR)

RNA extraction

Plants for RNA extracion were collected at ZT (Zeitgeber Time) between 2 and 4 from the start of the light period. RNA from Marchantia or *Arabidopsis* (*ca.* 100 mg) was extracted using the RNeasy plant mini kit (QIAGEN). To remove contaminating DNA, the TURBO DNAfreeTM Kit (Thermo Fisher Scientific) was used according to the manufacturer's recommendations. RNA samples were quantified using a NanoDrop ND-1000 spectrometer (Thermo Fisher Scientific). cDNA was synthesized from 0.5 μg or 1.0 μg of total RNA. Reverse transcription was performed in 25 μL with 20 μg/ml Oligo(dT) 12-18 primers and 200 units of SuperScript II Reverse Transcriptase (Thermo Fisher Scientific) according to the manufacturer's protocol. The resulting cDNA was diluted 1:9 with nuclease-free water. To control for genomic DNA contamination, control replicates of all samples were incubated without reverse transcriptase.

Primer tests and quantitative RT-PCR

Quantification was carried out using a 7500 Fast Real-Time PCR System (Applied Biosystem). Reactions were performed in 20 μL volumes containing 10 μL 2X SYBR Green mix (BioRad), 100 nM forward and reverse primers, and 1 μL diluted cDNA. Three technical and biological replicates were performed for each reaction. All relative expression levels were calculated following Livak et al.;[74] ubiquitin genes (At*UBQ10* At4g05320 and Mp*UBQ* Mp4g02740) were used as reference genes.[75] Primers for relative expression evaluation of Mp*BES1* in Marchantia and of brassinosteroid biosynthetic genes At*CPD (*At5g05690), At*CYP85A* (At3g30180) and At*DWF4* (At3g50660) in *Arabidopsis*, as well as reference genes, are listed in Table S1.

RNA sequencing and analysis

RNA from WT and *Mpbes1-2* mutant was extracted as described above. Poly-A mRNA libraries were prepared using "TruSeq Stranded mRNA Sample Prep Kit" (Illumina) from 1-2 ug of good quality RNA (R.I.N. > 7). Further purification steps were performed with 0.81X Agencourt AMPure XP beads. Final RNA libraries were quantified with Qubit 2.0 Fluorometer (Thermo Fisher Scientific). Libraries were then processed with Illumina cBot for cluster generation on flowcell and sequenced on paired-end (2x125bp, 30M reads per sample) at the multiplexing level requested on HiSeq2500 (Illumina). The CASAVA v1.8.2 of Illumina pipeline was used to process raw data and de-multiplexing. Raw reads were quality filtered and trimmed with a minimum score quality of 25 (Phred) and a minimum read length of 35bp using BBDuck software.

Dual luciferase transactivation assay for BR binding elements

The full length CDS of At*BZR1* (At1g75080) was amplified from cDNA by PCR using Q5 High-Fidelity DNA Polymerase (New England Biolabs) with attB-containing primers and introduced into pDONR201 (Thermo Fisher Scientific) vector using Gateway BP Clonase II Enzyme mix (Thermo Fisher Scientific). Primers used are listed in Table S1. At*BZR1* and Mp*BES1* coding sequences were introduced into pEarleyGate203[56] to generate effectors with N-terminal myc-tag fusions using Gateway LR Clonase II Enzyme mix (Thermo Fisher Scientific). The luciferase reporters carrying five concatemerized copies of the BRBE in the At*CPD* promoter were provided by Miguel A. Blázquez.[35] Agrobacterium suspensions were preincubated in a solution of half-strength MS, acetosyringone 100 μM, sucrose 0.5% at OD_{600nm} = 0.5, mixed at a ratio 1:3:1 (reporter: effector: silencing suppressor P19) and infiltrated in the abaxial surface of 4-week-old *N.benthamiana* leaves. After three days, soluble proteins from 30 mg of leaves were extracted using the Dual-Glo Luciferase Assay System (Promega) and quantified with an Infinite Lumi luminometer (Tecan). Three biological replicates were performed for each combination, and luciferase activities were recorded 30 minutes after the addition of the substrates.

Yeast one-hybrid assay

A fragment 500bp upstream of the start codon of At*CPD* was amplified from genomic DNA with primers containing XbaI and SacI sites and introduced into pTUY1H[57] by ligation. Prey coding sequences (At*BES1*, At*BZR1* and Mp*BES1*) were introduced into pDEST22 (Thermo Fisher Scientific) through Gateway LR recombination. Primers used are listed in Table S1. Bait and prey plasmids were introduced into *S.cerevisiae* Y187 (TakaraBio) by the lithium acetate/single-stranded carrier DNA/polyethylene glycol method as previously described[76] and transformants selected at 28°C in a synthetic defined medium lacking Leu and Trp [6.7g/l N base (TakaraBio), 20% (w/v) glucose (Sigma-Aldrich), dropout supplement -Leu/-Trp (TakaraBio) (pH 5.6), 1.5% (w/v) Phyto Agar (Duchefa)]. Selected colonies were grown overnight in the same liquid medium and spotted at OD_{600nm} = 1 on selective synthetic defined medium lacking Leu, Trp and His supplemented with 3-Aminotriazole (3AT, Sigma-Aldrich) as indicated. Images were taken after 3-5 days of growth at 28°C.

Yeast two-hybrid assay

The full length CDS of Mp*GSK* (Mp7g04170) and At*BIN* (At4g18710) were amplified from cDNA by PCR using Q5 High-Fidelity DNA Polymerase (New England Biolabs) with attB-containing primers and introduced into pDONR201 (Thermo Fisher Scientific) vector using Gateway BP Clonase II Enzyme mix (Thermo Fisher Scientific). The coding sequences of Mp*GSK* and At*BIN2* and those of Mp*BES1* and At*BES1* were introduced into pGBKT7-DEST and pGADT7-DEST, respectively, via Gateway LR recombination. Primers used are listed in Table S1. Yeast transformation was performed by lithium acetate/single-stranded carrier DNA/polyethylene glycol method as previously described.[76] Y2HGold (TakaraBio) yeast strain was transformed with pGADT7-DEST- and pGBKT7-DEST-derived expression vectors and selected in a synthetic defines medium lacking Leu and Trp. Selected colonies were grown

overnight in the same liquid medium and spotted at OD_{600nm} = 1 on selective synthetic defined medium lacking Leu, Trp and His supplemented with 3AT as indicated. Images were taken after 2-3 days of growth at 28°C.

Phosphorylation of BEH proteins

The full length CDS of At*BEH3* (At4g18890) was amplified from cDNA by PCR using Q5 High-Fidelity DNA Polymerase (New England Biolabs) with attB-containing primers and introduced into pDONR201 (Thermo Fisher Scientific) vector using Gateway BP Clonase II Enzyme mix (Thermo Fisher Scientific). At*BEH3* and At*BES1* coding sequence were introduced into pEarleyGate203[56] via Gateway LR (Thermo Fisher Scientific) recombination for N-terminal myc-tag fusions. At*BIN2* and Mp*GSK* coding sequences were introduced into pB7WGF2[59] via Gateway LR (Thermo Fisher Scientific) recombination for N-terminal eGFP fusions. Primers used are listed in Table S1. pEarleyGate203:Mp*BES1*, pEarleyGate203:At*BES1*, pEarleyGate203:At*BEH3*, pB7WGF2-At*BIN2* and pB7WGF2-Mp*GSK* plasmids were transformed into *Agrobacterium tumefaciens* GV3101 by electroporation. Agrobacterium suspensions were preincubated in a solution of half-strength MS, 100 μM acetosyringone and 0.5% sucrose at OD_{600nm} = 0.5, combined as indicated and infiltrated in the abaxial surface of 4-week-old *N.benthamiana* leaves. After 3 days, 50mg of the 5th and 6th leaves from the apical bud were collected, and processed for western blotting as described above. Myc-tag was detected with mouse anti-myc IgG (Sigma-Aldrich, 1:5000) and rabbit anti-mouse IgG coupled to peroxidase (Sigma-Aldrich, 1:5000); GFP was detected with anti-GFP serum (Thermo Fisher Scientific, 1:2000) and goat anti-rabbit IgG coupled to peroxidase (Sigma-Aldrich, 1:5000).

Brassinazole treatment

For brassinazole treatments (BRZ, Sigma-Aldrich, dissolved in dimethyl sulfoxide (DMSO)), seeds of the indicated genotypes were spotted regularly on MS plates supplemented with different BRZ concentrations. BRZ volumes were adjusted with solvent so that all plates had equal amounts of DMSO. Seeds were stratified at 4°C for 48h and induced to germinate with a two-hour white-light treatment. After 3 days in darkness at 22°C, seedlings (n = 15 for each genotype) were individually laid onto MS plates and scanned against a dark background. Hypocotyls were measured using ImageJ software.[62] The experiment was repeated twice with independent batches of seeds.

eBL and LiCl treatments

12-day-old *Arabidopsis* seedlings of the indicated genotypes, grown on MS-agar medium, were floated in MS liquid medium containing 1 μM epi-BL (eBL, Sigma-Aldrich, dissolved in 80% ethanol) or 10mM LiCl (Sigma-Aldrich) in the light. After 2 hours, 50mg of blotted dried seedlings were snap frozen in liquid N_2 and processed for western blotting as described above. AtBES1 and GFP were detected with anti-BES1 serum[8] and anti-GFP serum (Thermo Fisher Scientific, 1:2000) respectively, and revealed with goat anti-rabbit IgG coupled to peroxidase (Sigma-Aldrich, 1:5000).

QUANTIFICATION AND STATISTICAL ANALYSIS

General statistical analyses

Statistical analysis was performed using GraphPad Prism 8 (https://www.graphpad.com:443/). The values shown in the figures are either means of biological replicates or means of independent experiments, as specified in each figure caption. Details of statistical tests applied are indicated in figure legends including statistical methods, number of biological replicates, number of individuals, mean and error bar details, and statistical significances

RNA sequencing data analyses

Filtered reads were aligned to the *Marchantia polymorpha* v3.1 genome using STAR aligner (version 2.5.2b).[64] FeatureCounts (version 1.5.1) was used to get raw fragment counts.[65] Raw counts were then normalized using TMM method and low-counts genes and genes with high variability were filtered out using HSTfilter package in R.[67] Differential expression was calculated using edgeR package in R.[68]

Annotations on putative *Arabidopsis* homologs, GO categories and protein domains were retrieved from GFF files available at Phytozome (https://phytozome-next.jgi.doe.gov/pz/portal.html). GO enrichment analysis was performed based on categories available in the annotation file, using all features detected as background. Calculations and representations were performed in R with core functions and using TopGO package. To test for enrichment in homologs of AtBES1/AtBZR1 targets among deregulated genes in the Mp*bes1-2* mutant, the *Arabidopsis* best orthologs (as in the Marchantia annotation file) were intersected with high-confidence AtBES1 or AtBZR1 targets[28,29] and a Fisher's exact test was performed using all detected features as universe. To confirm that obtained p values were significant, we bootstrapped 100 times the test by randomly sampling from the Marchantia genome the same number of genes as were deregulated in the *Mpbes1-2* mutant.

Search for enrichment in *cis*-regulatory elements

A *de novo* search was performed using Homer v4.11 (http://homer.ucsd.edu/homer/motif/).[70] Sequences 500 bp upstream of the transcription start were retrieved from MpTak1 v5.1 genome (https://marchantia.info/download/tak1v5.1/) and the findMotifs.pl function was applied to the top 500 up- and 500 downregulated genes in *Mpbes1* knock-out mutant. Using promoters from all genes as background, motifs with a p value < 1E-13 were considered significantly enriched.